# Equatorial evening prereversal electric field enhancement and sporadic $E$ layer disruption: A manifestation of $E$ and $F$ region coupling

M. A. Abdu,[1] J. W. MacDougall,[2] I. S. Batista,[1] J. H. A. Sobral,[1] and P. T. Jayachandran[2]

[1] An investigation of the evening prereversal enhancement in the equatorial zonal electric field (PRE) based on ionosonde data show that the PRE development process is coupled with the sporadic $E$ layer formation in the evening over Fortaleza. Larger PRE amplitudes are associated with disruption of the $Es$ layer, whereas for smaller PRE amplitudes such disruption does not occur, in general. The $Es$ layer disruption does not occur also when the PRE amplitude decreases or is inhibited under a disturbance dynamo electric field. The disruption of these layers is followed by their reconstitution after a break of ∼3 hours. An examination of the relative role of the electric field and winds on ion velocity convergence process shows that the $Es$ layer formation from a shearing (or height-independent and westward) zonal wind is directly influenced by a vertical electric field (but not by zonal electric field). Measurements of the $Es$ patch zonal drift velocities by a digital ionosonde seem to support the role of a westward wind in the $Es$ layer formation. The observed association between the PRE and $Es$ layer disruption/formation is shown to arise from sunset-related vertical electric field development originating from the $E$ and $F$ region electrodynamic coupling processes. The results demonstrate the competing influences of the vertical electric field and the zonal wind in the evening $Es$ layer processes. Since the PRE is responsible for the equatorial spread $F$ (ESF) development, its relationship with the $Es$ layer is discussed in the context of the day-to-day variability of the ESF. *INDEX TERMS:* 2415 Ionosphere: Equatorial ionosphere; 2411 Ionosphere: Electric fields (2712); 2437 Ionosphere: Ionospheric dynamics; 2427 Ionosphere: Ionosphere/atmosphere interactions (0335); 2435 Ionosphere: Ionospheric disturbances; *KEYWORDS:* equatorial ionosphere, equatorial prereversal electric field, sporadic E-layer, E-layer winds, magnetic disturbances, E-F-region electrical coupling

## 1. Introduction

[2] The equatorial ionosphere and thermosphere constitute a coupled system whose phenomenology is controlled primarily by the electric field structure resulting from the interaction of the thermospheric wind, geomagnetic field, ionospheric plasma, and gravity. There are different aspects to the coupling processes and different ways in which they manifest themselves. The $E$ layer plasma confined to quasi-horizontal geomagnetic field lines is the seat of the electrojet current. The field lines higher up connect the equatorial $F$ region to conjugate $E$ layers, permitting strong electrical coupling of these regions. Field line mapped $E$ layer dynamo electric fields drive the plasma drift of the equatorial $F$ region, and the thermospheric winds of the $F$ region

establish field-aligned currents that could modify the driving ($E$ layer dynamo) electric field [*Rishbeth*, 1971; *Heelis et al.*, 1974]. The most observable effect of such coupled processes occurs at sunset when the rapid decay of field line integrated conductivity, into the night side, gives rise to an enhanced zonal (eastward) electric field arising from the $F$ layer dynamo driven by the thermospheric wind that blows eastward at these hours. This enhanced electric field, widely known as the prereversal enhancement electric field (PRE) [*Woodman*, 1970; *Fejer et al.*, 1991] has been modeled numerically [*Heelis et al.*, 1974; *Crain et al.*, 1993; *Batista et al.*, 1986; *Eccles*, 1998] as well as by the self-consistent NCAR thermosphere-ionosphere-electrodynamics general circulation model (TIEGCM) [*Fesen et al.*, 2000]. The PRE is basically responsible for the resurgence of the evening plasma fountain and the associated large uplift of the $F$ layer, which leads to instability development responsible for equatorial spread $F$/plasma bubble irregularity events. The PRE manifests longitude dependent seasonal variation as was demonstrated by *Abdu et al.* [1981]. Day-to-day variability in the thermospheric winds, in the $E$ layer

---

[1]Instituto Nacional de Pesquisas Espaciais (INPE), São José dos Campos, Brazil.
[2]University of Western Ontario, London, Canada.

tidal winds, and in the conductivity distributions, as well as the magnetic disturbance induced electric fields and winds, are directly responsible for the widely observed variability of the PRE, which is a principal cause of the observed day-to-day variability of equatorial spread $F$ occurrence.

[3] Another aspect of the coupling process concerns the expectation [*Cole*, 1996] that the gravity wave driven dynamo processes in the conjugate $E$ regions could provide the needed energy budget for field-aligned irregularities, including those that characterize plasma bubbles. Experimental observation by *Sastri* [1994] of $E$ region time scales in the evening $F$ region vertical drift fluctuations seems to support this theoretical expectation. There are also other important aspects of the dynamic and electrodynamic coupling of the $E$ and $F$ regions that need to be understood better. For example, the enhanced evening eastward electric field could cause plasma (and hence conductivity) depletion in the $E$ region, which primarily controls the development of that very electric field, thus leading to a potential source of day-to-day variability in this electric field (as pointed out by *Haerendel et al.* [1992]). We need to know also the effects of the changing winds of the $E$ region on the processes that couple the $E$ and $F$ region. Such information could help us understand better the causes of the day-to-day variability of the equatorial thermosphere-ionosphere phenomena and especially spread $F$.

[4] While the most readily observable manifestation of the thermospheric wind day-to-day variability perhaps resides in the variability observed in the PRE [see, e.g., *Rishbeth*, 1971; *Richmond*, 1995; *Abdu et al.*, 1995], an associated manifestation at $E$ layer heights had not been established. In this paper we show that sporadic $E$ layer phenomenology in the evening sector at locations in the vicinity of the magnetic equator (just outside the electrojet belt) appears to be a good candidate for such an investigation. A preliminary study by *Abdu et al.* [1996] suggested that the evening uplift of the $F$ layer over Fortaleza was associated with the disruption of the sporadic $E$ layer. This result posed some important questions such as (1) what is the role of the evening electric field enhancement on sporadic $E$ layer formation, or, conversely, what is the effect of the latter, through its possible modification of field line integrated conductivity, on the former? (2) Is there a vertical dynamic coupling process that forms the basis of a common driving force for the coupled changes in the evening $F$ layer height (PRE) and sporadic $E$ layer intensity, and (3) to what extent does the sporadic $E$ layer possibly influence the development of spread $F$ instabilities directly through its modification of the integrated conductivity of a potentially unstable field line and/or indirectly through its relationship with the sunset electric field of item 1? In this paper we address the first two questions. The result of the study will show that the mere presence of sporadic $E$ layers in the evening is by itself an unlikely direct cause of the observed day-to-day variability of the PRE. Rather, the development of the PRE could involve coupling processes that directly control $E_s$ layer development with the possibility of consequent electrodynamic and feedback effects. The study is based on data sets on $F$ layer heights and sporadic $E$ layer critical parameters collected during several campaign intervals (such as the Solar-Terrestrial Energy Program (STEP) and SUNDIAL international collaborative campaigns con-
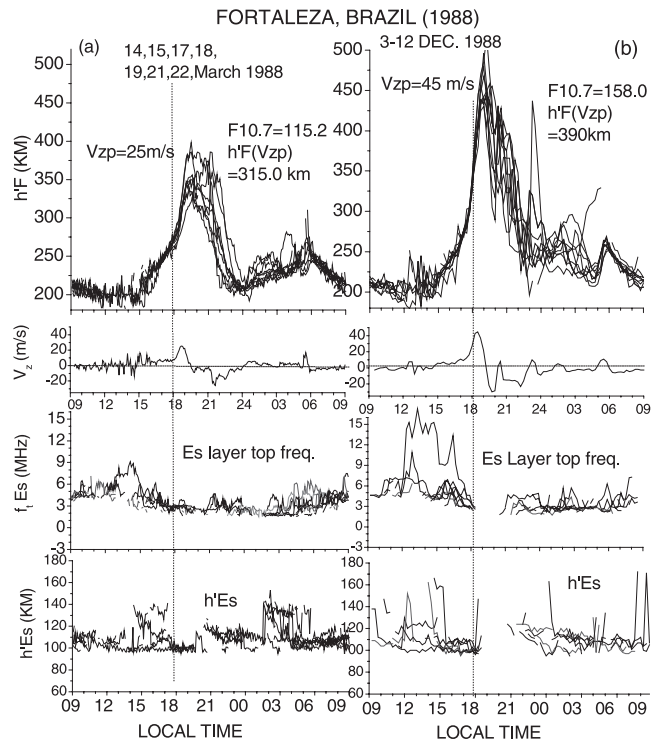


**Figure 1.** The $F$ layer base virtual height, $h'F$, at 5-min resolution mass plotted for a 7-day campaign interval in March 1988 and 10-day period in December 1988 (top); the vertical drift velocity $V_z = (dh'F/dt)$ based on the mean $h'F$ values (second); the top frequency scattered/reflected by the sporadic $E$ layer, denoted as $f_tE_s$ for the same set of days (third); $h'E_s$, the virtual height of the $E_s$ layer (bottom). A vertical line marks the time ($\sim$1800 LT) near which the $E_s$ layer disruption occurs as Figure 1b.

ducted during the past years) and additional periods of magnetically quiet and disturbed conditions. The solar flux parameter, F10.7, varied from an average of $\sim$115 to $\sim$250 for the data sets used in this study.

## 2. Results: Evening $F$ Layer Uplift and Sporadic $E$ Layer

[5] Fortaleza (3.9°S, 38.45°W, dip angle $-7°$ in 1988) is located in a region of a global maximum in secular variation in magnetic dip angle which corresponds to a variation in this parameter of $\sim$0.2° per year according to the International Geomagnetic Reference Field (IGRF). In the early 1970s this station was close to the equatorial electrojet (EEJ) center, with the dominant sporadic $E_s$ layer observed being the q-type ($E_{s-q}$ layer). With the shift away from the EEJ, sporadic $E$ layers of blanketing type, produced by ionization convergence arising from wind/wind shear effects have been observed in later years over Fortaleza [*Abdu et al.*, 1996]. The results presented here, which refers to the period 1988– 2001, correspond to this latter type of $E_s$ layer.

[6] Figure 1a presents, in the top panel, a plot of the height of the $F$ layer base, $h'F$, for a 7-day period during March 1988. The mean solar flux index (F10.7) for this

**Table 1.** Values of the Evening $F$ Region Prereversal Drift Velocity Peak ($V_{zp}$), the Solar Flux Unit F10.7, Their Standard Deviations (SD), and the $h'F$ for the $E_s$ Layer Disruption and Nondisruption Cases During the Three Intervals Analyzed

| Parameters | March 1988 Nondisruption | December 1988 Disruption | March–April 2001 Nondisruption | November–December 2001 Disruption | September–October 1989 Nondisruption | September–October 1989 Disruption |
|---|---|---|---|---|---|---|
| $V_{zp}$, m s$^{-1}$ | **25.0** | **45.0** | **37.0** | **62.0** | **40.0** | **48.0** |
| SD, m s$^{-1}$ | 7.6 | 4.5 | 13.1 | 13.6 | 11.6 | 13.0 |
| F10.7 | 115.2 | 158.0 | 178.1 | 214.0 | 200.8 | 241.2 |
| SD | 10.4 | 3.3 | 29.8 | 26.2 | 46.3 | 42.5 |
| $h'F$ at $V_{xp}$ | 315.0 | 390.0 | 360.0 | 500.0 | 367.0 | 376.0 |

period was 115.2. The most outstanding feature in this and in similar plots of Figure 1b is the rapid rise of the $F$ layer height around sunset (close to the vertical line shown at 1800 LT) caused by the enhanced zonal (eastward) electric field in the evening, the PRE, which is produced by the $F$ layer wind dynamo at sunset hours. The relationship between this height increase and the concurrent $E_s$ layer behavior is the focus of this paper. The vertical drift velocity $V_z$ of the layer determined as $d(h'F)/dt$ is shown in the second panel. The velocity so determined should be close to the real $F$ region vertical plasma drift for layer height $\geq$300 km [*Bittencourt and Abdu*, 1981; *Batista et al.*, 1985], which usually is the case during evening hours. The evening peak velocity $V_{zp}$ that occurs near 1900 LT has a mean value of 25 m s$^{-1}$ for the group of days of Figure1a, the corresponding mean $h'F$ being 315 km. The third panel (from top) of Figure 1a shows the top frequency reflected and/or backscattered by the $E_s$ layer (that is, $f_tE_s$, sometimes also denoted as $f_xE_s$). The $f_tE_s$ shows a broad daytime maximum and nighttime minimum; note that the $E_s$ layer continues through sunset and night hours. This result contrasts with that of Figure 1b, which shows similar plots, but for the interval 3–12 December 1988, with mean F10.7 = 158.0. The rapid rise of the $F$ layer at sunset, due to the PRE, for this group of days is significantly larger than for the case of March 1988. The mean $V_{zp}$ for this case is 45 m s$^{-1}$ (as per the plot in the second panel) with the corresponding $h'F$ = 390 km, both being significantly larger than their corresponding values for March 1988. It is interesting to note that in this case at the time of the large height rise, around 1800 LT, the $E_s$ layer formation is disrupted to start again after ~3 hours. The mean $V_{zp}$ and F10.7 values with their standard deviations (SD) and the mean $h'F$ values for this and two other cases to be discussed below are given in Table 1.

[7] The differences of the $V_{zp}$ and F10.7 values between the $E_s$ layer disruption and nondisruption cases are significantly larger than their respective SD values. Thus the results in Figures 1a and 1b suggest a clear association between the sunset $F$ layer height rise and $E_s$ layer disruption, the larger vertical drift velocity and therefore $F$ layer height being associated with $E_s$ layer disruption. The bottom panels of Figures 1a and 1b present the virtual height, $h'E_s$, of the sporadic $E$ layers, corresponding to the data plotted in the third panel. The $h'E_s$ often shows a descending trend lasting for several hours, both in Figures 1a and 1b, suggesting that the velocity shear nodes of a tidal wind pattern are responsible for these $E_s$ layers. The descending feature is not always evident, however.

[8] Similar results from analysis of more recent data collected during the year 2001 are presented in Figure 2.

In this case the data was separated into two groups, one in which the evening $E_s$ layer disruption took place very close to 1800 LT (2100 UT) and the other in which such disruption did not occur. The $V_{zp}$ values for the $E_s$ layer disruption and nondisruption cases in these data sets are 62 m s$^{-1}$ 37 m s$^{-1}$, respectively, their difference being significantly larger than the standard deviations for each group (Table 1). The corresponding mean $F$ layer heights near $V_{zp}$ are ~360 km and ~500 km, respectively. These results, corresponding to an epoch of relatively higher solar flux values, strongly support the behavior inferred from Figure 1.

[9] The data from a campaign conducted in September–October 1989, corresponding to an epoch close to solar maximum with average F10.7 = 220 was subjected to similar analysis and the results are shown in Figures 3a and 3b. The mean $V_{zp}$ for the two groups of days in this case are 40 m s$^{-1}$ and 48 m s$^{-1}$, the corresponding $h'F$ being 367 km and 376 km, respectively. These results do show that the $E_s$ layer is disrupted when statistically the $F$ layer
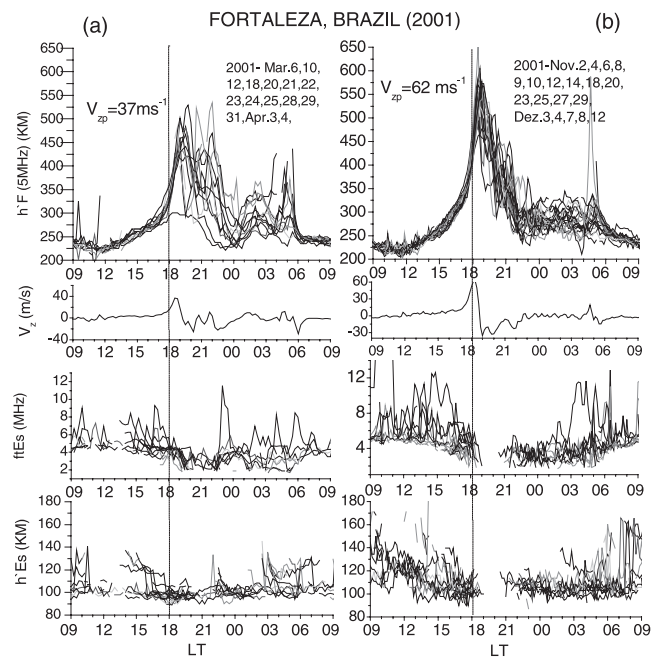


**Figure 2.** $F$ layer height versus $E_s$ layer relationship similar to that of Figure 1, but for more extended periods during March–April and November–December 2001. (left) the case of postsunset $E_s$ layer nondisruption; (right) the case of $E_s$ layer disruption. (Note the large difference between the values of $V_{zp}$ for the two cases).
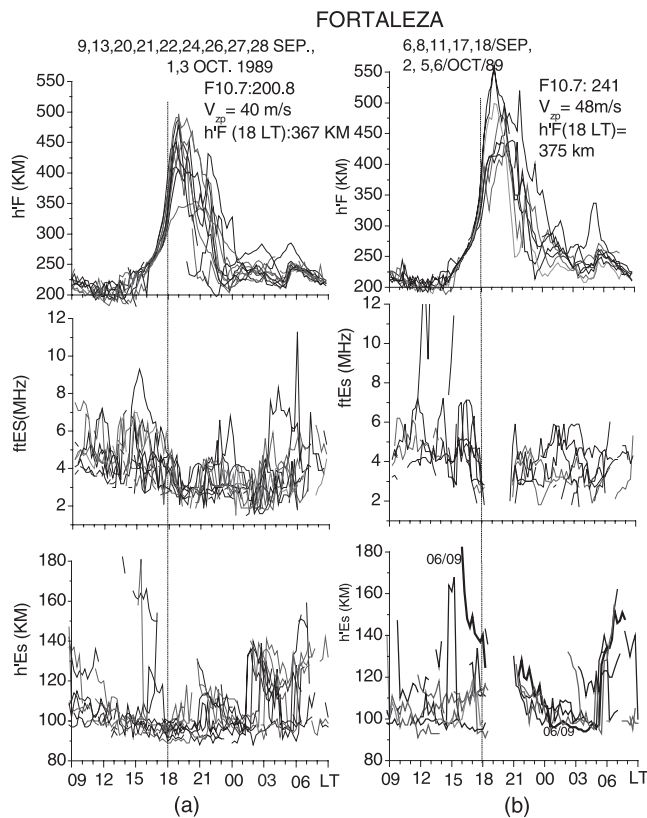
**Figure 3.** (a) Mass plots of $h'F$ (top), $f_tE_s$ (middle), and $h'E_s$ (bottom) for a group of days, selected during a campaign in September–October 1989 for which sporadic E layer was not disrupted at sunset (b) Similar plot as in Figure 3a but for a different group of days for which the $E_s$ layer disruption occurred at ∼1800 LT to start again after ∼2.5 hours.

vertical drift velocities (and therefore $h'F$) are larger, for a range of F10.7 representing high solar flux conditions. It may be noted that the differences in $V_{zp}$ and $h'F$ values for these $E_s$ layer disruption and nondisruption cases are smaller than in Figures 1 and 2. The differences in $V_{zp}$ and the corresponding F10.7 values are in fact smaller than or comparable to the SD for the two groups as shown in Table 1. In view of the well-known positive dependence of $V_{zp}$ on the F10.7 [Fejer et al., 1991] the results of Figure 3 are in reasonably good agreement with those of Figures 1 and 2. Further, the results of Figure 3 suggest a more complex solar flux dependence of the observed effect. A precise relationship with the solar flux needs to be established from a considerably more extensive data set than has been possible in the present study. The $h'E_s$ plotted in the bottom panel of Figure 3 also shows descending trends lasting a few hours. Particularly noteworthy is an event in Figure 3b of 6 September (marked 06/09 on Figure 3b) when a descending $E_s$ layer that began at ∼1600 LT and at ∼180 km persisted until morning hours and <100 km. During its descent the layer underwent disruption at ∼1800 LT and reformation at ∼2100 LT, the layer height always remaining at what looks like the descending nodal point of a wind shear. We have analyzed a few more data sets from campaigns conducted during 1991–1992. The

results corroborate the above findings in all aspects and are not presented here.

[10] The association between the $E_s$ layer disruption and the evening $F$ layer height rise is evident also in a few cases examined under magnetically disturbed conditions. An example is presented in Figure 4 which shows, during the interval, 17–19 September 1979, the $h'F$ and $h'_3F$ (the $F$ layer virtual height at 3 MHz) variations in the top panel. (The thin dotted line represents a reference curve, which is the mean of the $h'F$ variation for the 5 quietest days of the month). The corresponding $E_s$ layer critical frequencies are plotted in the middle panel. The bottom panel shows the variations in AU and AL indices on these days. On the evening of 17 September, which was clearly under quiet conditions with no preceding auroral disturbances (at least for a day), there is a significant $F$ layer height rise at sunset (indicated by a vertical line at 1800 LT) as expected for a quiet time PRE (with $V_{zp} = 70$ m s$^{-1}$). During this $F$ layer rise the $E_s$ layer is disrupted, which is consistent with the effects demonstrated in Figures 1, 2, and 3. A series of substorms occurred starting at ∼2000 LT (2300 UT) on 17 September which continued till the afternoon of 18 September. The F layer rise on the evening of 18 September is observed to be small (with $V_{zp} = 25$ m s$^{-1}$) as compared with its large rise on the previous evening. As a result the $E_s$ layer formation on this evening was uninterrupted, in agreement with results shown before. On the evening that followed (clearly undisturbed) the pattern returned to a normal one of $F$ layer height rise and the associated $E_s$ layer disruption (with $V_{zp} = 41$ m s$^{-1}$). Sobral et al. [1997] have studied some other aspects of these disturbed intervals. Results for other case studies of disturbed intervals show agreements with these findings. Thus the pattern of large
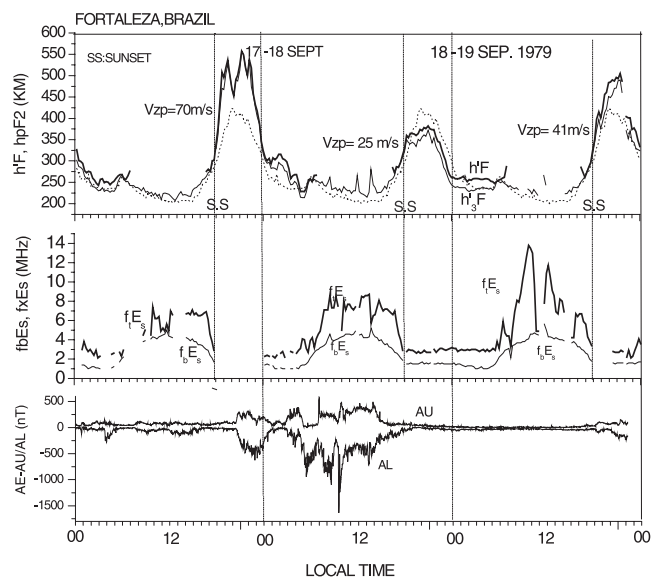


**Figure 4.** (top to bottom) $h'F$ and $h'_3F$ (the virtual height of the 3 MHz plasma frequency), $f_xE_s$ (equivalent to $f_tE_s$) and $f_bE_s$ (the blanketing frequency of the $E_s$ layer) and the auroral activity indices, AU and AL, plotted during 17–19 September 1979. SS = sunset. See the text for further explanation.

(small) $F$ layer rise and associated $E_s$ layer disruption (nondisruption), seen in the individual cases associated with magnetically disturbed conditions, are in complete agreement with the results from the statistical data sets representative of "undisturbed" intervals presented before.

## 3. Discussion

[11] The association between the two phenomena, the fast evening $F$ layer rise and sporadic $E$ layer disruption and reformation, seems to be clearly established in these results. In an attempt to understand the possible cause of such an association we need to consider the mechanisms known to operate for the two phenomena. The $F$ layer evening uplift is caused by the PRE, known to result from the $F$ layer wind dynamo that dominates at these hours, as first proposed by *Rishbeth* [1971]. Owing to the day-to-night decrease of the $E$ layer conductivity that establishes itself as a strong longitudinal gradient across the sunset terminator, a significantly reduced loading of the $F$ region electric field by $E$ region conductivity occurs toward the nightside. Under such a situation the action of an eastward thermospheric wind in the $F$ region can produce, by dynamo action, vertical (downward) electric field increasing toward the nightside, which leads to the enhanced zonal (eastward followed by westward) electric field. The PRE development was originally modeled on principles of electrical coupling between the $E$ and $F$ layers by *Heelis et al.* [1974]. The precise explanation of this electric field enhancement seems to involve different but interrelated processes. The basic relationship between the $F$ region dynamo vertical electric field and the zonal electric field that constitute the PRE arise from a curl-free requirement for electric field as proposed by *Rishbeth* [1971]. However, the PRE seems to involve other distinct contributions as well. *Farley et al.* [1986] have shown that a zonal electric field enhancement could arise from charge collection in the off-equatorial $E$ region resulting from the divergence of Hall current, which is driven by the $F$ region downward polarization field (resulting from the wind dynamo) mapped down to the conjugate $E$ regions. *Haerendel and Eccles* [1992] proposed the Cowling conductivity gradient (dropping towards night) in the EEJ at sunset, which requires enhanced zonal electric fields involving vertical currents and an $F$ region dynamo current system on the nightside, as contributing to the development of the PRE. Briefly, the main basic mechanism can be considered to operate as follows. Thermospheric zonal winds produce, by dynamo action, a vertical polarization field in the $F$ region whose magnitude is dependent upon field line integrated conductivities. If $\Sigma_S$ is the Pedersen conductivity integrated along the segment of a field line in the $F$ region (considered as source region) and $\Sigma_L$ is that integrated along the same field line for the segments extending into the conjugate $E$ regions (considered as load region) the $F$ region vertical polarization electric field $E_z$ can be represented by the following relationship:

$$E_z = U_y \times B_0 \left[ \frac{\Sigma_S}{\Sigma_L + \Sigma_S} \right]. \qquad (1)$$

$U_y$ is the thermospheric zonal wind and $B_0$ is the magnetic field intensity (considered positive westward and north-

ward). It is easy to verify from equation (1) that during daytime when the load region conductivity $\Sigma_L$ (of the $E$ layer) is large (that is, $\Sigma_L \gg \Sigma_S$) $E_z$ tends to be zero, as to be expected. At postsunset hours $\Sigma_L$ decays faster than $\Sigma_S$ thus contributing to the development of a vertical electric field whose intensity increases towards the nightside (that is, across the terminator). The application of the curl-free condition to such an electric field variation could result in the enhanced evening zonal electric field, the PRE, recently modeled by *Eccles* [1998] [see also *Rishbeth*, 1971]. From considerations underlying the coupling processes it is evident that the magnitude and local time structure of the zonal wind as well as that of the longitudinal conductivity gradient across the terminator could control the amplitude and phase of the PRE [see, e.g., *Batista et al.*, 1986; *Crain et al.*, 1993; *Abdu et al.*, 1995].

[12] The sporadic $E$ layer of interest in this study is the low-latitude blanketing type. The blanketing frequency could often be below the usual observable limit of an ionosonde ($<\sim$1.5 MHz). Both the blanketing frequency ($f_bE_s$) and the top frequency reflected/scattered by the layer (denoted as $f_tE_s$ or $f_xE_s$) are used as indicators of the presence, absence, or relative strength of the layer. Such layers are produced by the well-known wind shear mechanism [*Whitehead*, 1961; *Axford*, 1963; *Nygren et al.*, 1984; *Mathews*, 1998]. At lower heights ($<$120 km) vertical shear in the zonal wind is the most efficient mechanism of $E_s$ layer formation. At even lower heights (100–105 km region) even a height independent westward wind is capable of producing $E_s$ layers as was shown by *Abdu and Batista* [1977]. Even though the tidal mode $E_s$ layers show descending patterns from higher than 140 km down to $\sim$100 km, statistically most of these $E_s$ layers remain for relatively longer times between $\sim$100 and $\sim$110 km, sometimes they could peak around 105 km, and in Figures 1–3 they were located mostly in the 95–120 km height region.

[13] In light of the mechanisms briefly described above, an attempt to understand the observed association between the PRE and the sporadic $E$ layer formation would need to address the following questions as to a possible cause-effect relationship:

[14] 1. Does the $E_s$ layer presence in the evening modify the $E$ layer integrated conductivity and hence its longitudinal gradient to the extent necessary to modify the evening prereversal electric field enhancement and therefore the $F$ layer uplift? If so, is it possible that the $E_s$ layer variability could be thought of as a primary cause of the observed association between the two phenomena?

[15] 2. Alternatively, do the processes that are known to be responsible for the $F$ layer height rise (explained before) influence also the formation of the $E_s$ layers at these hours? If so, does the enhanced evening electric field control the $E_s$ layer formation?

[16] Regarding question 1, the results presented in Figures 1–4 do not seem to provide any obvious indication of a possible effect on the $F$ layer uplift by the mere presence of the evening $E_s$ layer. For example in the results of Figure 1a for March 1988, the evening $E_s$ layer disruption did not take place; the associated evening $F$ layer vertical drift ($V_{zp}$) and the corresponding height were 25 m s$^{-1}$ and $\sim$315 km, respectively. In contrast, in Figure 3a for September–October 1989 the $E_s$ layer interruption also did not take

place but these values were significantly higher: 40 m s$^{-1}$ and ~367 km, respectively. (Similar argument applies to Figure 2a as well). Such increases can be due to the solar flux dependent (and to a lesser degree seasonal) effects [*Fejer et al.*, 1991]. Another point to be noted is that the sunset increases in $V_z$ and $h'F$ begin at local times earlier than the $E_s$ layer interruption that usually takes place near 1800 LT (or a little later), as can be verified by comparing the results in Figures 1–3. A still better argument is that in Figures 1, 2, and 3 the $E_s$ layer critical frequency is about the same for both the higher and lower $V_{zp}$ values. These points would seem to suggest that the degree of sunset $F$ region vertical drift and height, that is, the $F$ layer dynamo intensity, does not show a direct dependence on the mere $E_s$ layer presence/interruption, based on the present data set. Results from case studies involving responses during magnetic disturbances presented in Figure 4 lead to a similar inference. The cases of decreased PRE under disturbed condition, such as that observed on 18 September 1979, is believed to be produced by a disturbance dynamo westward electric field [*Blanc and Richmond*, 1980; *Scherliess and Fejer*, 1997; *Abdu et al.*, 1997] and/or by an associated disturbance zonal (westward) wind [*Abdu et al.*, 1995]. There is no evidence that the occurrences of the decreased PRE are controlled by the simple persistence of $E_s$ layers. On the contrary, the PRE development process seems to influence the $E_s$ layer formation, as we shall discuss.

### 3.1. Roles of Zonal Wind and Electric Field in Vertical Ion Velocity Convergence for $E_s$ Layer Formation

[17] In order to examine the points related to question 2 above, we consider below the relative importance of neutral winds and electric fields in the $E_s$ layer formation. A general expression for the vertical ion velocity $v_z$ arising from external force terms driven by wind and electric field components in the east-west, north-south, and vertical directions [see, e.g., *Banks and Kockarts*, 1973], can be manipulated to yield a simple expression that represents only effects from zonal and vertical electric fields and zonal winds valid for Fortaleza (dip angle $I = -9°$), that is, for latitudes just off the magnetic equator. Using a coordinate system with the x-axis horizontal and towards magnetic north, the y-axis westward and the z-axis upward, the vertical ion velocity is given by:

$$v_z = \frac{R_i}{1 + R_i^2}\left[\frac{E_z}{B_0} - \frac{E_y}{B_0}\frac{X}{R_i} - U_y X + U_x Z X\right], \quad (2)$$

where $R_i = \frac{\nu_i}{\Omega_i}$; $X = \frac{B_x}{B_0}$; $Z = \frac{B_z}{B_0}$; $B_o$, $B_x$, and $B_z$ are the total magnetic field intensity and its x and z components, respectively; $\nu_i$ = collision frequency of ions with neutrals; $\Omega_i$ = ion gyro frequency assumed constant in the height regions of interest here; $E_y$, $E_z$ are the zonal and vertical electric fields, respectively; $U_x$ and $U_y$ are the meridional and zonal winds, respectively. For the Fortaleza latitude $X \cong 1$ and $Z \ll 1$ and therefore the contribution from meridional winds can be neglected. Thus the vertical ion velocity is approximately

$$v_z = \frac{R_i}{1 + R_i^2}\left[\frac{E_z}{B_0} - \frac{E_Y}{B_0 R_i} - U_y\right]. \quad (3)$$

The contribution from all terms except from $E_y$ has maximum effect at $R_i = 1$ (around 130 km). Equations for $dv_z/dz$, the vertical convergence of vertical ion velocity, responsible for the layer formation are given below for three height regions:

Case (a): $(R_i^2 \gg 1, h < 120$ km)

$$\frac{dv_Z}{dz} = \frac{1}{R_i}\left[-\frac{E_z}{B_0 H_n} + \frac{d}{dz}\frac{E_z}{B_0} + \frac{U_y}{H_n} - \frac{d}{dz}U_y\right] + \frac{E_y}{B_0}\frac{2}{R_i^2 H_n}, \quad (4)$$

Case (b): $(R_i = 1, h \cong 130$ km)

$$\frac{dv_Z}{dz} = \frac{1}{2}\left[\frac{d}{dz}\frac{E_Z}{B_0} - \frac{d}{dz}U_Y + \frac{E_Y}{B_0 H_n}\right], \quad (5)$$

Case (c): $(R_i^2 \ll 1, h > 135$ km)

$$\frac{dv_Z}{dz} = R_i\left[\frac{E_Z}{B_0 H_n} + \frac{d}{dz}\frac{E_Z}{B_0} - \frac{U_Y}{H_n} - \frac{d}{dz}U_Y\right], \quad (6)$$

where $H_n = R_i/(dR_i/dz)$ is the neutral scale height, and $h$ is the height. (These equations were derived by assuming $E_y$ to be height independent, and they will not be valid for dip angles smaller than ~±0.6°). The maximum efficiency of $E_s$ layer formation represented by equation (5) occurs in the 130 km region. For case (c), $R_i^2 \ll 1$, the small effects from all terms in equation (6) becomes negligible with increase in height, the layer formation becoming inefficient above ~150 km for typical values of $U_y$, $E_z$, and their height gradients.

[18] We may note from equation (4) that in the height region of most interest (120 km and below) the direct contribution from $E_y$ to $E_s$ layer formation becomes negligibly small. Thus the $E_s$ layer formation results from the competing/complementary influences of $E_z$ and $U_y$ and their vertical gradients. Using these equations, a realistic evaluation of $E_s$ layer disruption/reformation would require precise knowledge of the local time and height structure of $E_z$ and $U_y$ in the evening sector $E$ region. However, such information is lacking, especially for the latitude of Fortaleza. We shall therefore use some available theoretical/model results for these parameters to evaluate their competing influences on the PRE associated $E_s$ layer phenomenon.

### 3.2. Vertical Electric Field Structure of the Evening Equatorial Ionosphere

[19] The vertical electric field of the equatorial ionosphere arises from different sources [see, e.g., *Richmond*, 1973; *Haerendel et al.*, 1992]: (1) The zonal electric field of the $E$ layer dynamo driving downward Hall current that produces a polarization charge and upward field line perpendicular electric fields, basically responsible for the electrojet current; (2) the zonal (eastward) wind dynamo in the evening that drives upward directed current mainly in the $F$ region [*Rishbeth*, 1971] producing a downward polarization field which does not completely offset the vertical current; (3) a net upward current associated with 2 being accounted by the divergence of the horizontal (elec-trojet) current as explained by *Haerendel et al.* [1992]. Following *Haerendel et al.* [1992] who used field line integrated parameters the
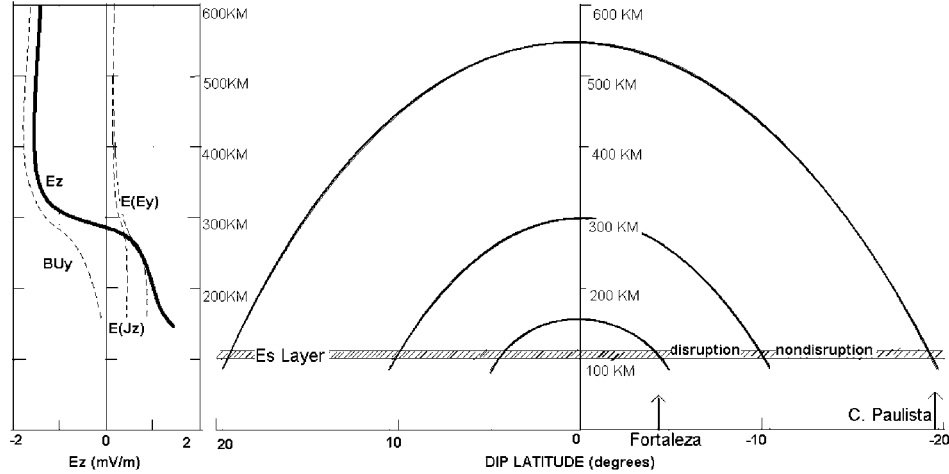
**Figure 5.** (left) Height profiles of vertical electric field $E_z$ (also denoted as $E_L$ in the text) at 1900 LT as per the model based on rocket observation over Natal, Brazil adopted from *Haerendel et al.* [1992]. The symbols identifying the curves represent the component of $E_z$ arising from: zonal wind, $BUy$, zonal electric field, $E(E_y)$, vertical current $E(J_z)$, and the total field $E_z$. (right) Magnetic field line mapping the $E_s$ layer height over Fortaleza and Cachoeira Paulista on to the equatorial plane.

vertical electric field $E_z$, consisting of the above three components, can be represented as:

$$E_z = -\frac{\Sigma_H}{\Sigma_P}E_Y + B(L)U_y^P + \frac{J_z}{\Sigma_P}. \qquad (7)$$

$U_y^P$ is the Pedersen conductivity weighted value of $U_y$, $\Sigma_{H,P}$ is the field line integrated Hall and Pedersen conductivities, $J_z$ is the net upward current from the $E$ region, and $B(L)$ is the magnetic field intensity as a function of its "$L$" value. (Equation (1) is a simplified form of equation (7) when the effect from zonal wind only is considered, and note that westward is positive). Using one-dimensional solutions of equation (7) and other coupled equations, *Haerendel et al.* [1992] determined the typical height structure of $E_z$ (denoted as $E_L$ in their paper) for equinoctial (September) sunset conditions over Natal, Brazil. Part of their results for 1900 LT (from their Figure 8) is adopted in Figure 5 which shows that the net $E_z$ is directed upward below $\sim$300 km and downward above, consistent with the sheared plasma flow of the evening lower $F$ region, being westward below and eastward above this height as observed by different researchers [*Kudeki et al.*, 1981; *Tsunoda et al.*, 1981]. At an $E$ layer height of 105 km over the latitude of Fortaleza (4° dipole latitude), which maps in the equatorial plane to $\sim$136 km, the $E_z$ is upward, and from Figure 5, should be of the order of 2 mV/m. $E_z$ can vary significantly from one evening to the other due to the variability in all the terms of equation (7).

### 3.3. On the Relative Importance of $E_z$ and $U_y$ in Vertical Ion Velocity Convergence

[20] Equations (3) and (4) can be used to determine the relative contributions from the zonal wind and vertical and zonal electric fields to the vertical ion velocity and its vertical convergence, within the height region of the dominant $E_s$ layers considered here. Table 2 shows the values of $v_z$ and $dv_z/dz$, arising from the different terms of

equations (3) and (4) calculated for the Fortaleza latitude and assuming typical values for various parameters, which are also shown.

[21] In the case of $v_z$ values arising from the three terms of equation (3) as listed in Table 2, it can be noted that the contribution from the zonal electric field is very small compared with those from the zonal wind $U_y$ and vertical electric field $E_z$. Such a small vertical ion velocity arising from the zonal electric field at these heights, where $R_i$ has large values, is in agreement with the results of *Hanson et al.* [1983]. The values of $dv_z/dz$ in Table 2 do not include contributions arising from vertical gradients in wind and electric fields, which (especially in the case of winds) could often be more significant than that of the height independent terms (those with $1/H_n$).

[22] A negative ion velocity gradient is necessary to produce the ionization convergence that forms a sporadic $E$ layer. From equation (4) we see that (independent of the presence of wind shear or vertical electric field) a steady height-independent westward zonal wind (the third term on the right side) can produce a negative vertical gradient in vertical ion velocity and hence ionization convergence. As was shown earlier by *Abdu and Batista* [1977] a westward steady wind of 100 m s$^{-1}$, would correspond to $dv_z/dh$ of

**Table 2.** Vertical Ion Velocity, $v_z$, and its Vertical Gradient, $dv_z/dz$, Calculated Using Typical Values of Their Control Parameters as Discussed in the Text for Three Heights[a]

| Height | $R_i/1 + R_i^2$ | $v_z$, m s$^{-1}$ | | | $dv_z/dz$,[b] m s$^{-1}$/km | |
| | | $E_z/B_0$ | $U_y$ | $E_y/R_iB_0$ | $E_z/B_0H_n$ | $U_y/H_n$ |
|---|---|---|---|---|---|---|
| 100 km | 0.052 | 5.2 | −5.2 | −.137 | .88 | −.88 |
| 105 km | 0.099 | 9.9 | −9.9 | −.49 | 1.67 | − 1.67 |
| 110 km | 0.148 | 14.8 | −14.8 | − 1.12 | 2.52 | −2.52 |

[a]$U_y = 100$ m s$^{-1}$; $E_y = 1$ m vm$^{-1}$; $E_y/B_0 = 50$ m s$^{-1}$; $E_z = 2$ mV/m, $E_z/B_0 = 100$ m s$^{-1}$; $H_n = 6.0$ km; I = 9°.
[b]Only contributions from terms with $H_n$ are included here.

$\sim$1m s$^{-1}$/km which is capable of producing an $E_s$ layer with peak density enhancement by a factor of 1.5−2 for an ambient ionization density of $5 \times 10^{10}$−$10^{11}$ m$^{-3}$. From the values of Table 2 (the last two columns) it is evident that a negative velocity gradient produced by such a wind can be annulled by a vertical electric field of 2 mV/m which could, as per equation (4), thus disrupt the formation of an $E_s$ layer. (For the present discussion we assume that the contribution from gradients in $E_z$ can be assumed to be small). The wind amplitude such as that considered above is usually of a tidal mode as is seen in the descending pattern of these $E_s$ layers (Figures 1−3). In this case the $E_s$ layering can occur at the null point of a vertical shear, characterized by a positive vertical gradient in the zonal wind, that is, a westward wind above and an eastward wind below a null point. A null point of vertical shear in zonal wind arising from a dominant tidal component can be observed near 105 km during late afternoon hours in TIEGCM simulation results on sequential $E_s$ layer occurrence patterns over Australia [*Wilkinson et al.*, 1992].

### 3.4. Observational Evidence on the Possible Role of a Westward Wind on $E_s$ Layer Formation

[23] Indication of the dominant role of a westward wind in the formation of an $E_s$ layer has been obtained from measurements of $E_s$ layer drift velocities by a Canadian Advanced Digital Ionosonde (CADI) [*Grant et al.*, 1995] operated at Fortaleza. The zonal velocity of $E_s$ layer patches at 100−105 km, as measured by the CADI, can be used as a proxy for the zonal wind. The CADI utilizes the Doppler spectra of the echoes received by spaced receivers to determine the zonal velocity. As the value of $R_i$ at this height range varies from $\sim$10 to $\sim$20, even if the magnitude of the zonal drift so obtained is an underestimate of the zonal wind, the direction of its velocity should be correct. Figure 6 presents, as examples, three cases (presented in three pairs of panels) of layer height and zonal velocity variations over Fortaleza measured by the CADI. The upper panel of each pair shows the layer heights, $h'E_s$ and $h'F$, at 5-min intervals, and the lower panel shows the zonal drift velocities at 2-min interval. For these measurements the height sampling by the CADI was limited to <150 km to select the $E_s$ layer drift velocity.

[24] For all the three cases the velocity, which is partially westward in the afternoon, turns clearly westward near sunset and then shows a steady and significant increase toward the nightside, which coincides with the rise in the $F$ layer height due to the PRE. These results support our contention based on equation (3) that a westward wind can be a driving force in the formation of these layers. In all the three cases the westward velocity reached the order of 70−80 m s$^{-1}$ before the layer is disrupted. The local time of such disruption is different on the different days, which may be related to the different rates of $h'F$ increases on these days. We may note also that the westward drift velocity increases at different rates on theses days.

### 3.5. Possible Mechanism of $E_s$ Layer Disruption and Reformation

[25] In the absence of sufficient information on the local time and height structure of the vertical electric field over Fortaleza, our attempt below to explain the phenomenon
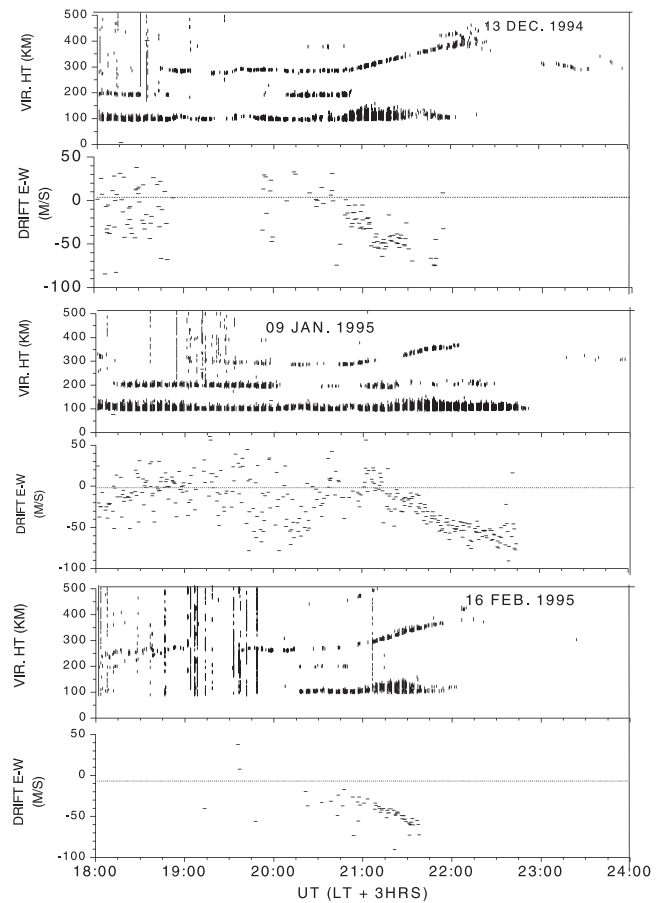


**Figure 6.** The top two panels show plots of the layer height (virtual height at 3 MHz) at 5-min resolution and zonal drift velocity at 2-min resolution (positive eastward), respectively, in the upper and lower panels, measured by a CADI over Fortaleza on 13 December 1994. The middle two panels are similar plots but for 9 January 1995, and the lower most two panels are for 16 February 1995.

assumes that an $E_s$ layer formed from a tidal zonal wind is in place just when the evening vertical electric field enhancement begins to develop. The possible effect of imposing an $E_z$ on an ongoing $E_s$ layer is then examined. A simple one-dimensional model is used to calculate the effect of a semidiurnal tidal wind on the electron density and Pedersen conductivity in the height region of 90−140 km using slabs of 1/2 km and time steps of 5 s. The assumption inherent in such a one-dimensional model is that variations in any horizontal direction are insignificant. The model was initiated with a uniform density of $5 \times 10^{11}$ /m$^3$ at all heights within the height interval considered. The recombination of molecular ions follows the equations given by *Rishbeth and Garriott* [1969]. The electron production rate was set at $1 \times 10^5$/m$^3$ s$^{-1}$ at all heights, and diffusion terms were included. The vertical ion movement due to an imposed zonal wind was based on equation (3) (with $E_y = E_z = 0$) with $\nu_i$ from Appendix B of *Kelley* [1989], and $\Omega_i = 132$ rad s$^{-1}$. The semidiurnal wind field has a vertical wavelength of 50 km, and the amplitude, the same at all heights, was varied for different simulations. The phase of the wind was set so that

there is a null at 105 km at time $t = 0$ with westward wind above 105 km and eastward below. The model calculates the vertical ion motion as a function of height, and from the height gradient of the vertical motion the density variations were calculated

[26] The electron density height versus time variation that resulted for zero amplitude of the applied wind is plotted as isodensity lines in the top panel of Figure 7 from $t = 0$ to $t = 6$hrs. For this case the electron density decay under the postsunset conditions becomes monotonically faster at lower altitudes. The density variations obtained with a wind of 100 m s$^{-1}$ amplitude are shown in the middle panel, and the pattern of the wind field at 105 km is shown in the bottom panel. The null point of the wind field is shown as descending dashed lines in the middle panel. In the presence of the wind the electron density decay becomes faster above ~110 km than below where the $E_s$ layer development begins. Descending downward, the layer becomes well defined near 105 km within about $t = 1$ hour. Although the layer peak-to-ambient density ratio could continue to develop further, as the layer descends the densities begins to decay due to recombination [*MacDougall et al.*, 2000]. However, such decay may not occur in reality due to the possible presence of significant amount of metallic ions at these heights [see, e.g., *Narcisi*, 1968; *Mathews*, 1998]. It is pertinent to note that the height of the density peak of the $E_s$ layer remains above that of the wind null point, their separation increasing as the layer descends. The layer thus moves into a region of larger westward wind. The increasing westward velocity after sunset seen in the CADI zonal drift plots of Figure 6 may thus be accounted for.

[27] The development of sunset vertical electric field enhancement at E layer heights can get intense enough to affect an ongoing ion velocity convergence. According to equation (4), an upward electric field opposes the effect of zonal westward wind (or that of a positive wind shear) to cause vertical ion velocity convergence. (For the time being we ignore any possible effect from a vertical gradient in $E_z$). As pointed out in section 3.3, the effect of an electric field of 2 mV/m, which seems to be within the expected limits for the Fortaleza latitude (as per Figure 5), could counteract the ion convergence produced by a zonal westward wind of ~100 m s$^{-1}$ thus disrupting an ongoing wind-driven $E_s$ layer formation. This point was checked by performing test runs of our model by including invariant values of vertical electric field of 2 mV/m directed upward or downward in the height region of our calculation. The upward directed electric field produced an upward displaced $E_s$ layer with a considerably reduced peak density that could demonstrate the disruption of the $E_s$ layer as observed by our instruments. The effect of a downward electric field was a downdrafting of the ionization from higher level resulting in $E_s$ layer intensification. Additionally, according to equations (3)–(6), the competing/complementary effects from the prevailing vertical gradients in $E_z$ and in $U_y$ could modify the process either to expedite or retard the disruption process. We thus suggest the development of vertical electric fields under sunset electrodynamics processes to be the main factor responsible for the $E_s$ layer disruption observed over Fortaleza. Additional evidences in support of this suggestion are given below:
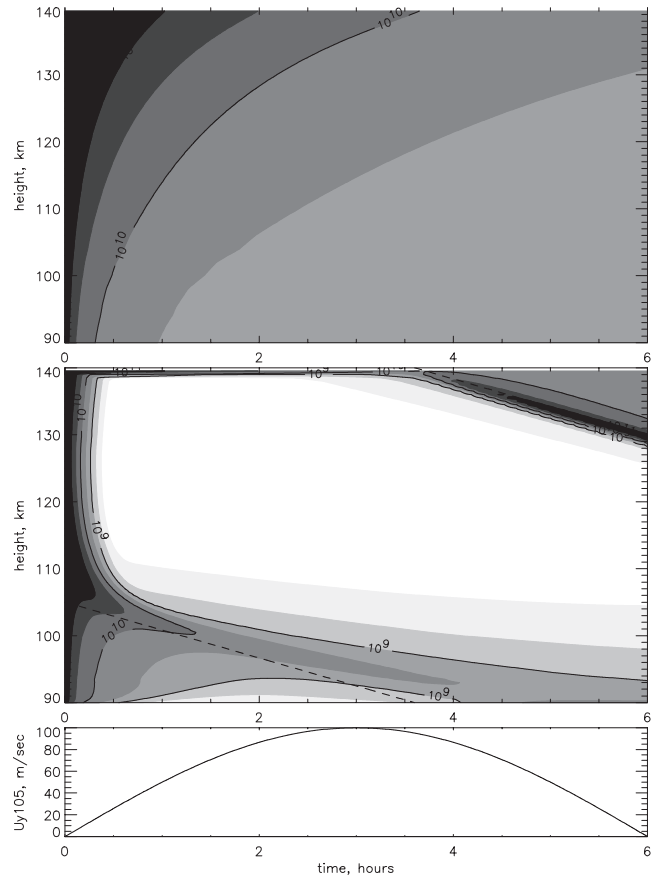


**Figure 7.** One dimensional simulation results, from $t = 0$ to $t = 6$ hours of (a) isoelectron density lines showing the decay of ionization at different heights when zonal wind is neglected (top), (b) when a zonal wind of 100 m s$^{-1}$ amplitude is included (middle), and (c) the zonal wind pattern at 105 km (bottom).

[28] 1. If an upward electric field is capable of disrupting an ongoing $E_s$ layer formation, then a reversal to downward of this electric field should favor its formation or even intensification. For example, in the region of 570 km over the equator which maps down to an E layer height of 105 km over Cachoeira Paulista (dip latitude $-15°$), the vertical electric field is ~$-2$ mV/m (downward, see Figure 5), which is expected to favor the $E_s$ layer formation according to equation (4). Figure 8 shows $E_s$ layer parameters over Cachoeira Paulista for the same group of days as in Figure 1b, and the uninterrupted $E_s$ layer occurrence (during the postsunset hours) over this station is in direct contrast to the $E_s$ layer disruption over Fortaleza. Thus while the upward electric field in the E region over Fortaleza (field line mapped to ~136 km over the equator) causes disruption of the $E_s$ layers, the downward electric field over Cachoeira Paulista region (field line mapped to ~570 km over the equator) causes uninterrupted formation. In this way, the simultaneous $E_s$ layer absence (presence) over Fortaleza (Cachoeira Paulista) corresponding to upward (downward) vertical electric field (referred to lower and higher heights in the equatorial plane) is consistent with the role of vertical electric fields
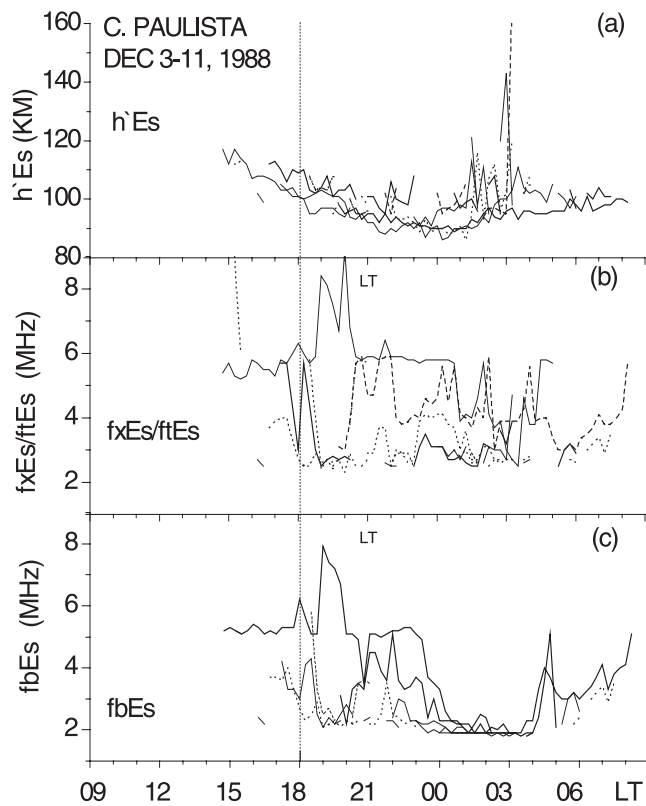
**Figure 8.** $E_s$ layer parameters, $h'E_s$, and $f_tE_s$ and $f_bE_s$ plotted in three panels for Cachoeira Paulista for the same days as in Figure 1b for Fortaleza.

in the PRE-associated $E_s$ layer behavior discussed in this paper. Many such examples have been noted also from examination of more recent simultaneous data from Fortaleza and C. Paulista (though not presented here).

[29]  2. The results of Figure 4 showing $E_s$ layer non-disruption in the evening that followed a magnetic disturbance seems to provide further independent evidence for the role of vertical electric fields on $E_s$ layer formation. In this case the zonal electric field enhancement (the $F$ layer uplift) is inhibited in the evening following a magnetically disturbed period. It is known that such inhibition can be caused by a westward electric field arising from the disturbance dynamo that develops over low latitudes within $5-8$ hours after the magnetic storm energy input over the auroral region [*Blank and Richmond*, 1980; *Abdu et al.*, 1997; *Scherliess and Fejer*, 1998]. A westward electric field, in this case arising from the disturbance dynamo, could produce downward electric field as per the first term of equation (7) [see also *Abdu et al.*, 1998]. The effect of such an electric field would tend to cancel that of the otherwise normally upward vertical electric field responsible for the quiet-time $E_s$ layer disruption, thus explaining the uninterrupted occurrence of the $E_s$ layer in association with an inhibited PRE.

[30]  The simulation results of Figure 7 produces a second cycle of ion convergence that appears near $t = 4$ hour at the next descending wind null. The decreasing $h'E_s$ of the reconstituted layers seen in Figures $1-3$ near 2100 LT corresponds to this situation. By this time the

postsunset zonal electric field turns westward, and vertical electric field downward (at all heights) [*Haerendel et al.*, 1992] with the resulting downward plasma transport favoring the $E_s$ layer reconstitution. Thus one-dimensional model results in combination with considerations of the local time and height structure of the evening vertical electric field seem to offer an explanation for the evening $E_s$ layer disruption, and its eventual reappearance, that occur in association with the evening uplift of the $F$ layer as observed over Fortaleza.

[31]  Figure 9 shows the height-integrated Pedersen conductivity versus time variation calculated by our model from $t = 0$ to $t = 6$ hours for different amplitudes of the wind field: 0, 20 m s$^{-1}$, 50 m s$^{-1}$ and 100 m s$^{-1}$. It may be noted that a westward wind produces significant modification to the rate and shape of the postsunset conductivity variation with respect to its zero wind pattern. Independent of the effect of vertical electric fields (not included in the model) the model results show that a faster westward wind produces a faster postsunset conductivity decay rate. (The increase in conductivity starting at $t = 4$ hrs corresponds to the reappearance of the descending $E_s$ layer below $\sim$140 km, seen in Figure 7). The different conductivity decay rates depending upon the wind velocities, seen in Figure 9, do in fact signify correspondingly different local time and therefore longitudinal gradients in conductivity that could in turn influence the PRE. It may be noted that since the wind field effective at $E$ layer heights (over Fortaleza) is part of a tidal wind its effect will be present over a large area extending to the $E$ region (farther poleward) that is linked to the $F$ region over Fortaleza. Therefore the results of Figure 9 that show an earlier and larger rate of change of conductivity for larger westward winds would suggest, as per equation (1), a modified local time/longitude variation of the evening vertical electric field, which, through application of curl-free conditions, could result in an earlier onset of an enhanced PRE. In other words, a larger westward wind in the $E$ layer could contribute to enhancement of the PRE, through processes involving vertical electric field development, as explained before, which in turn could contribute to the disruption of the zonal wind driven $E_s$ layer formation (dependent on latitude). Thus the efficiency of $E_s$ layer formation by a zonal (westward) wind near sunset seems to be impaired also by this electrodynamic feedback effect. Such an effect may seem to be a secondary one but merits consideration in any quantitative evaluation of the problem. Based on the aforementioned ideas, a simplified representation of the relevant coupling processes is shown in Figure 10. In this figure the box SS.$\Delta\Sigma$ represents the sunset-related local time/longitudinal gradient in field line integrated conductivity. The effect of $E$ region depletion arising from the PRE (represented by a separate box) is to be considered in conjunction with this (dash-dotted arrow). Other boxes use known symbols used elsewhere in the text. The figure is self-explanatory and solid arrows show the basic/well-known coupling paths and dotted arrows indicate the mechanism suggested for the $E_s$ layer disruption/reformation processes. The basic driving forces for the $E_s$ layer formation/disruption are shown by the links with the boxes containing $E_z$, $U_y$, and $dU_y/dz$. A possible effect of the $E_s$ layer ionization on the PRE through contribution to the longitudinal gradient in the field line integrated conductivity
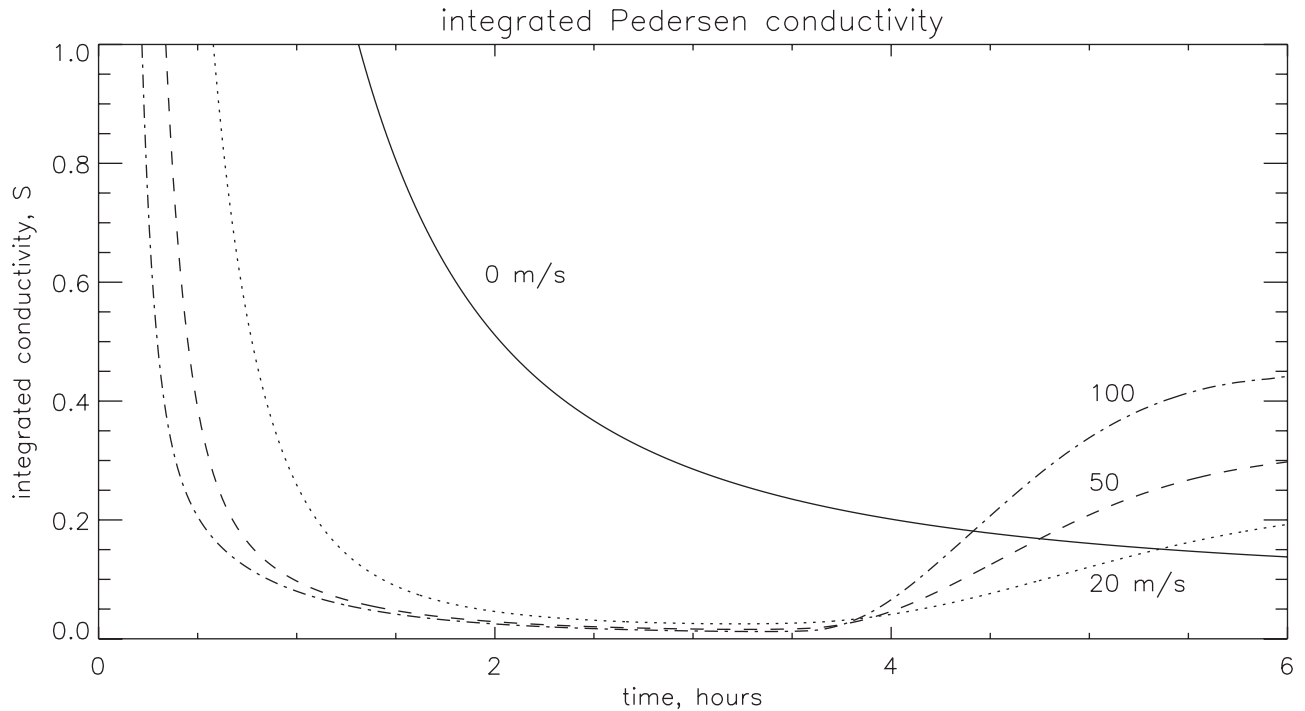
integrated Pedersen conductivity



**Figure 9.** One-dimensional simulation results of height integrated Pedersen conductivity in unit of S (Siemens) as a function of time for zonal (westward) wind amplitudes 0 m s$^{-1}$, 20 m s$^{-1}$, 50 m s$^{-1}$, and 100 m s$^{-1}$.

is also shown (by dashed line). The feed back effect characterized by the postsunset $E$ layer conductivity depletion contributing to intensification of the prereversal enhancement of the eastward electric field which in turn enhances the conductivity depletion [*Haerendel and Eccles*, 1992] can be visualized in the figure. The resulting $E$ layer conductivity variation has an interesting consequence not explicitly shown in this block diagram. The faster decay rate with increasing height of the postsunset $E$ layer conductivity (that is, the decay rate being faster above ~120 km than below) provides a situation which could lead to development of a vertical electric field (as per equation (1)) under the action of a zonal wind/wind shear required for the $E_s$ layer formation. The zonal wind/wind shear can thus become (in yet one more way) a less efficient driver of the $E_s$ layer (as per equations (3) and (4)).

[32] It is pertinent to point out here that the role of vertical electric fields on the $E_s$ layer formation as presented here would imply existence of distinct latitudinal belts of interrupted, or enhanced, evening $E_s$ layer occurrence based on the vertical structure of the evening vertical electric field. For example, on the basis of vertical electric field structures as determined by *Haerendel et al.* [1992] (Figure 5) we could expect a zone of uninterrupted evening $E_s$ layer occurrence at latitudes higher than ~9°. As we saw earlier the uninterrupted/enhanced evening $E_s$ layer occurrence over Cachoeira Paulista (dip lat −15°) is consistent with this expectation. The poleward limit of this zone is not clearly defined. The latitudinal belt defined by lat <~9° is the zone of evening $E_s$ layer disruption. Its equatorward limit seems to be a few degrees (2−3°) away from the center of the EEJ at which the blanketing $E_s$ layer formation might become operative. These points, however,

need to be tested further when additional/suitable data becomes available.

[33] The PRE that causes the evening uplift of the $F$ layer is a pre requisite for spread $F$/plasma bubble instability generation. The higher the amplitude of this electric field the more intense could be the resulting spread $F$ event [see, e.g., *Abdu*, 2001; *Abdu et al.*, 1983; *Fejer et al.*, 1999]. We see that a smaller amplitude of the PRE that could weaken, if not inhibit, the spread $F$ instability growth is also the condition that permits the continuation of evening $E_s$ layer
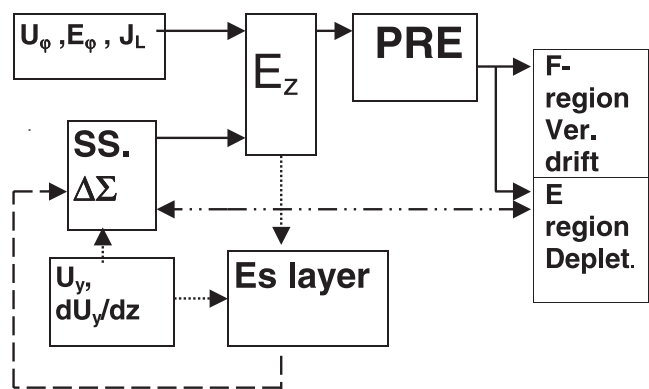


**Figure 10.** A schematic of the processes associating the PRE and the sporadic $E$ layer disruption and reformation. The boxes connected by solid lines/arrows represent the well-known processes for the PRE. The box connections by dotted and dashed lines represent the proposed schemes involved in the $E_s$ layer disruption and reformation processes.

formation (within the relevant latitude range), through reduced vertical electric field. In fact the association between the PRE/spread $F$ and the $E_s$ layer has two aspects: one of them resides in the coupling processes that underlie the PRE-$E_s$ layer connection that we have focused in this paper; the other aspect concerns the possible direct effect of the $E_s$ layer ionization on the field line integrated conductivities and hence in the ESF instability growth rate [see, e.g., *Stephan et al.*, 2002]. An evaluation of possible ESF-$E_s$ layer connection needs to consider both of these aspects. It will be of great value to include the effect of latitude-dependent $E_s$ layer features in electrodynamics simulations of the evening equatorial ionosphere aiming at clarifying questions on the widely observed quiet-time variabilities in PRE and ESF phenomena. $E_s$ layer observations at suitably selected conjugate locations coupled with the knowledge of the associated $E$ layer winds should be reckoned as important elements in the investigation of the sunset electrodynamics leading to spread $F$ development.

## 4. Conclusions

[34] The main findings from this study can be summarized as follows. In the immediate vicinity of the magnetic equator but outside the direct influence of the equatorial electrojet, sporadic $E$ layers are produced by vertical shears in zonal winds as well as by height-independent zonal winds. Their formation can be disrupted, however, during the vertical uplift of the $F$ layer that occurs at sunset hours due to the action of the prereversal electric field enhancement produced by the $F$ layer dynamo. It is observed that in general and for specific periods, the amplitude of the PRE is clearly larger when $E_s$ layer disruption occurs as compared with cases when such disruption does not occur. Such a relationship between the PRE and $E_s$ layer disruption is observed also under conditions of disturbance electric fields and winds that follow magnetic storms. Considerations of the vertical ion motion under external forcing by electric fields and neutral winds show that the ion convergence leading to $E_s$ layer formation processes is controlled mainly by zonal wind/wind shear and vertical electric field, with little effect from zonal electric field. The zonal drift measurement carried out by a CADI shows association of the $E_s$ layer with westward drift/wind, the latter increasing in amplitude as a precursor to the $E_s$ layer disruption during the postsunset hours. Based on our present understanding of the sunset electrodynamics processes leading to the development of the PRE it can be inferred that larger amplitude of thermospheric zonal wind and associated larger postsunset vertical and zonal electric field enhancements are conditions propitious for the $E_s$ layer disruption as compared with their smaller amplitudes when such disruption does not take place. The observational data do not provide a clear indication of any possible direct effect of the $E_s$ layer ionization (such as through the field line integrated conductivity) on the development of the PRE although this possibility could exist and merits further investigation. A one dimensional simulation shows that the zonal (westward) wind responsible for the $E_s$ layer formation also produces modified local time/longitudinal gradients in height integrated conductivity in the postsunset hours, which could in turn modify the development of the PRE, thus providing a possible (secondary) source of PRE variability from $E$ layer winds. The model helps visualize the $E_s$ layer formation through the action of a tidal zonal wind and its disruption through imposition of a postsunset vertical electric field. Owing to the lack of information on the precise local time and vertical structure of the vertical electric field our model did not include vertical electric fields except in test runs performed to check the effects of fixed values of such electric fields. An important point regarding the evening $E_s$ layer disruption is that it occurs under the competing/complementary conditions of zonal wind/wind shear and vertical electric field. The reappearance of the $E_s$ layers after a break of ~3 hours often at a higher altitude (than where the disruption occurred) is consistent with the results of simulation. The circumstance of possible enhancement of the background ionization owing to the reversal of the PRE electric fields at these times that could contribute to the resumption of the $E_s$ layer was verified by the model. The suggested latitudinal structuring of the $E_s$ layer disruption and non disruption zones, though based on observations at two stations only, seems to be consistent with what is expected from the known height structure of the vertical electric field and appears to provide additional support to our explanation of the role of vertical electric fields in the observed evening $E_s$ layer behavior. Our proposed explanation is also supported by the $E_s$ layer nondisruption cases observed under disturbed conditions. Further investigations of these problems aiming at better clarification of the causes of the well-known day-to-day variability of the PRE versus $E_s$ layer and equatorial spread $F$ development are in progress.

## References

Abdu, M. A., Outstanding problems in the equatorial ionosphere-thermosphere electrodynamics relevant to spread $F$, *J. Atmos. Sol. Terr. Physics*, *63*, 869–884, 2001.

Abdu, M. A., and I. S. Batista, Sporadic $E$ layer phenomena in the Brazilian geomagnetic anomaly: Evidence for a regular particle ionization source, *J. Atmos. Terr. Phys.*, *39*, 723–731, 1977.

Abdu, M. A., J. A. Bittencourt, and I. S. Batista, Magnetic declination control of the equatorial $F$ region dynamo field development and spread $F$, *J. Geophys. Res.*, *86*, 11,443–11,446, 1981.

Abdu, M. A., R. T. Medeiros, J. H. A. Sobral, and J. A. Bittencourt, Spread $F$ plasma vertical rise velocities determined from spaced ionosonde observations, *J. Geophys. Res.*, *88*, 9197–9204, 1983.

Abdu, M. A., I. S. Batista, G. O. Walker, J. H. A. Sobral, N. B. Trivedi, and E. R. de Paula, Equatorial ionospheric electric field during magnetospheric disturbances: Local time/longitude dependence from recent EITS campaigns, *J. Atmos. Terr. Phys.*, *57*, 1065–1083, 1995.

Abdu, M. A., I. S. Batista, P. Muralikrishna, and J. H. A. Sobral, Long-term trends in sporadic $E$ layers and electric fields over Fortaleza, Brazil, *Geophys. Res. Lett.*, *23*, 757–760, 1996.

Abdu, M. A., J. H. Sastri, J. MacDougall, I. S. Batista, and J. H. A. Sobral, Equatorial disturbance dynamo electric field, longitudinal structure, and spread $F$: A case study from GUARA/EITS campaigns, *Geophys. Res. Lett.*, *24*, 1707–1710, 1997.

Abdu, M. A., P. T. Jayachandran, J. W. MacDougall, and J. H. A. Sobral, Equatorial $F$ region zonal plasma irregularity drifts under magnetospheric disturbances, *Geophys. Res. Lett.*, *25*, 4137–4140, 1998.

Axford, W. I., The formation and vertical movements of dense ionized layers in the ionosphere due to neutral wind shears, *J. Geophys. Res.*, *68*, 769, 1963.

Banks, P. M., and G. Kockarts, *Aeronomy*, Academic, San Diego, Calif., 1973.

Batista, I. S., M. A. Abdu, and J. A. Bittencourt, Equatorial F region vertical plasma drift: Seasonal and longitudinal asymmetries in the American sector, *J. Geophys. Res.*, *91*, 12,055, 1986.

Bittencourt, J. A., and M. A. Abdu, A theoretical comparison between apparent and real vertical ionization drift velocities in the equatorial *F* region, *J. Geophys. Res.*, *86*, 2451–2455, 1981.

Blanc, M., and A. D. Richmond, The ionospheric disturbance dynamo, *J. Geophys. Res.*, *85*, 1669–1689, 1980.

Cole, K. D., Equatorial thermosphere-ionosphere-plasmasphere disturbances, *J. Geomagn. Geoelectr.*, *48*, 187–210, 1996.

Crain, D. J., R. A. Heelis, G. J. Bailey, and A. D. Richmond, Low-latitude plasma drifts from a simulation of the global atmospheric dynamo, *J. Geophys. Res.*, *98*, 6039–6046, 1993.

Eccles, J. V., Modeling investigation of the evening prereversal enhancement of the zonal electric field in the equatorial ionosphere, *J. Geophys. Res.*, *103*, 26,709–26,719, 1998.

Farley, D. T., E. Bonelli, B. G. Fejer, and M. F. Larsen, The prereversal enhancement of the zonal electric field in the equatorial ionosphere, *J. Geophys. Res.*, *91*, 13,723–13,728, 1986.

Fejer, B. G., E. R. de Paula, S. A. Gonzalez, and R. F. Woodman, Average vertical and zonal plasma drifts over Jicamarca, *J. Geophys. Res.*, *96*, 13,901–13,906, 1991.

Fejer, B. G., L. Scherliess, and E. R. de Paula, Effects of the vertical plasma drift velocity on the generation and evolution of equatorial spread F, *J. Geophys. Res.*, *104*, 19,854–19,869, 1999.

Fesen, C. G., Crowley, R. G. Roble, A. D. Richmond, and B. G. Fejer, Simulation of the pre-reversal enhancement in the low latitude vertical ion drifts, *Geophys. Res. Lett.*, *27*, 1851–1854, 2000.

Grant, I. F., J. W. MacDougall, J. M. Ruohoniemi, W. A. Bristow, G. J. Sofko, J. A. Koehler, D. Danskin, and D. André, Comparison of plasma flow velocities determined by the ionosonde Doppler drift technique, SuperDARN radars, and patch motion, *Radio Sci.*, *30*, 1537–1549, 1995.

Haerendel, G., and J. V. Eccles, The role of the equatorial electrojet in the evening ionosphere, *J. Geophys. Res.*, *97*, 1224–1243, 1992.

Haerendel, G., J. V. Eccles, and S. Çakir, Theory of modeling the equatorial evening ionosphere and the origin of the shear in the Horizontal plasma flow, *J. Geophys. Res.*, *97*, 1209–1223, 1992.

Hanson, W. B., S. Sanatani, and T. N. L. Patterson, Influence of the E region dynamo on equatorial spread F, *J. Geophys. Res.*, *88*, 3169–3173, 1983.

Heelis, R. A., P. C. Kendall, R. J. Moffet, D. W. Windle, and H. Rishbeth, Electrical coupling of the E and F regions and its effect on the F region drifts and winds, *Planet. Space Sci.*, *22*, 743–756, 1974.

Kelley, M. C., *The Earth'sIonosphere: Plasma Physics and Electrodynamics*, Academic, San Diego, Calif., 1989.

Kudeki, E., B. G. Fejer, D. T. Farley, and H. M. Ierkic, Interferometric studies of equatorial F region irregularities and drifts, *Geophys. Res. Lett.*, *8*, 377–380, 1981.

MacDougall, J. W., J. M. C. Plane, and P. T. Jayachandran, Polar cap sporadic *E*: 2, Modeling, *J. Atmos. Sol. Terr. Phys.*, *62*, 1169–1176, 2000.

Mathews, J. D., Sporadic *E*: Current views and recent progress, *J. Atmos. Sol. Terr. Phys.*, *60*, 413–435, 1998.

Narcisi, R. S., Process associated with metal-ion layers in the *E* region of the ionsphere, *Space Res.*, *360*, 1968.

Nygren, T., I. Jalonen, J. Oksman, and T. Turunen, The role of electric field and neutral wind direction in the formation of sporadic E layers, *J. Atmos. Terr. Phys.*, *46*, 373–381, 1984.

Richmond, A. D., Equatorial electrojet 1, Development of a model including winds and instabilities, *J. Atmos. Terr. Phys.*, *35*, 1083, 1973.

Richmond, A. D., Modeling equatorial ionospheric electric fields, *J. Atmos. Terr. Phys.*, *57*, 1103–1115, 1995.

Rishbeth, H., Polarization fields produced by winds in the equatorial *F* region, *Planet. Space Sci.*, *19*, 357–369, 1971.

Rishbeth, H., and O. K. Garriott, *Introduction to Ionospheric Physics*, *Int. Geophys. Res.*, vol. 14, Academic, San Diego, Calif., 1969.

Sastri, J., Short period (5–33 min) variations in the vertical drift of F region plasma near the magnetic equator, paper presented at the STEP symposium, SCOSTEP, Sendai, Japan, 1994.

Scherliess, L., and B. G. Fejer, Storm time dependence of equatorial dynamo zonal electric filed, *J. Geophys. Res.*, *107*, 24,037–24,046, 1997.

Sobral, J. H. A., M. A. Abdu, W. D. Gonzalez, B. T. Tsurutani, I. S. Batista, and C. de Gonzalez, Effects of intense storms and substroms on the equatorial ionosphere/thermosphere system in the American sector form ground-based and satellite Data, *J. Geophys. Res.*, *102*, 14,305–14,313, 1997.

Stephan, A. W., M. Colerico, M. Mendillo, B. W. Reinisch, and D. Anderson, Suppression of equatorial spread F by sporadic E, *J. Geophys. Res.*, *107*(A2), 1021, doi:10.1029/2001JA000162, 2002.

Tsunoda, R. T., R. C. Livingstone, and C. L. Rino, Evidence of a velocity shear in bulk plasma motion associated with the postsunset rise of the equatorial F layer, *Geophys. Res. Lett.*, *8*, 807–810, 1981.

Wilkinson, P. J., E. P. Szuszczewicz, and R. G. Roble, Measurement and modeling of intermediate, descending, and sporadic layers in the lower ionosphere: Results and implications for global-scale ionospheric-thermospheric studies, *Geophys. Res. Lett.*, *19*, 95–98, 1992.

Whitehead, J. D., The formation of the sporadic *E* layer in the temperate zone, *J. Atmos. Terr. Phys.*, *20*, 49, 1961.

Woodman, R. F., Vertical drift velocities and east-west electric filed at the magnetic equator, *J. Geophys. Res.*, *75*, 6249–6259, 1970.

—————————
M. A. Abdu, I. S. Batista, and J. H. A. Sobral, Instituto Nacional de Pesquisas Espacias (INPE), 12201 970 São José dos Campos, Brazil. (abdu@dae.inpe.br; inez@dae.inpe.br; sobral@dae.inpe.br)

P. T. Jayachandran and J. W. MacDougall, Department of Electrical Engineering, University of Western Ontario, London, Canada N6A 3K7. (jaya@danlon.physics.uwo.ca; jmacdoug@uwo.ca)